

Seismic retrofitting of URM masonry piers with helical steel reinforcement

Szymon Cholostiakow¹, Brett McKinley², Panagiotis Mergos³, Christian Hall⁴, Andreas Kappos⁵,
Ashraf Ayoub⁶.

¹ Marie Curie Experienced Fellow, University of Thessaly, Volos, Greece.

Email: simon.cholost@gmail.com

 <https://orcid.org/0000-0001-8908-5888>.

² Lecturer; University of Central Lancashire, Preston, UK; formerly: Senior Lecturer; City University of London, London, UK.

Email: bmckinley@uclan.ac.uk

³ Senior Lecturer; City University of London, London, UK

Email: panagiotis.Mergos.1@city.ac.uk

 <https://orcid.org/0000-0003-3817-9520>

⁴ Technical Director; Target Fixings Ltd, Unit 3, Red Shute Hill Ind. Est., Hermitage RG18 9QL, UK.

Email: christianhall@targetfixings.co.uk

⁵ Professor and Faculty Lead in Structures; Khalifa University, Abu Dhabi, UAE

Email: andreas.kappos@ku.ac.ae

 <https://orcid.org/0000-0002-5566-5021>

⁶ Professor of Structural Engineering; City University of London, London, UK

Email: ashraf.ayoub.1@city.ac.uk

 <https://orcid.org/0000-0002-2670-9662>

Abstract: Past earthquakes revealed that brittle nature of unreinforced masonry (URM) structural walls often leads to extensive cracking and shear damage, which can seriously affect structural integrity and thus compromise the safety of the entire building. Hence, finding an effective seismic retrofitting solution that can increase the safety of existing masonry building stock is of great importance. This paper explores the potential of alternative seismic retrofitting solutions for URM masonry walls - near-surface mounted austenitic stainless-steel helical bars. Being cold rolled from a plain round wire and subsequently tensioned through a free-twisting process, such a reinforcement can not only offer high durability, but also superior mechanical and bond properties, as well as effective redistribution of loads through the retrofitted masonry. In addition, the relatively high flexibility of the bars allows them to be mounted continuously along the joints of the wall, leaving the aesthetic of the retrofitted masonry intact. A total of nine single-leaf clay brick walls were tested under cyclic displacement reversals to examine the seismic performance of the reinforcement in terms of increasing in-plane shear capacity and ductility. Test specimens comprised cantilever walls having various retrofitting patterns, including flexural and shear helical reinforcements installed in the mortar joints or into the vertical slots cut into the masonry. The results showed considerable improvements in the ductility and energy dissipation of the walls after the retrofitting. The paper highlights the potential of helical stainless-steel bars as a seismic retrofitting reinforcement capable of preserving the structural integrity of masonry structures at increasing displacement demands without affecting the aesthetic of the surface of the walls.

Keywords: Helical stainless-steel reinforcement, twisted bars, seismic retrofitting, masonry, in-plane damage, shear

1. Introduction

1 Unreinforced masonry (URM) buildings constitute more than 70% of the existing building
2 stock worldwide and make up the vast majority of the world's cultural and architectural heritage
3 [1]. Although masonry buildings have proven to be highly durable structures, much of the
4 [1]. Although masonry buildings have proven to be highly durable structures, much of the
5 existing building stock comprises non-engineered URM buildings, often built using weak
6 existing building stock comprises non-engineered URM buildings, often built using weak
7 materials and designed according to simple principles with little or no seismic provisions. The
8 materials and designed according to simple principles with little or no seismic provisions. The
9 in-plane behaviour of URM walls has been studied experimentally by many researchers, whose
10 in-plane behaviour of URM walls has been studied experimentally by many researchers, whose
11 work largely contributed to the current state-of-the-art [2-6]. Owing to its inherent non-
12 work largely contributed to the current state-of-the-art [2-6]. Owing to its inherent non-
13 homogeneity, the seismic behaviour of masonry under combined shear and compression loads
14 homogeneity, the seismic behaviour of masonry under combined shear and compression loads
15 is different from that of homogeneous materials. In general, the failure mode of URM walls
16 is different from that of homogeneous materials. In general, the failure mode of URM walls
17 subjected to in-plane seismic excitations depends on wall aspect ratio and axial load and is
18 subjected to in-plane seismic excitations depends on wall aspect ratio and axial load and is
19 characterised as either flexure controlled or shear controlled [6, 7]. For slender walls, with
20 characterised as either flexure controlled or shear controlled [6, 7]. For slender walls, with
21 relatively low axial loads, failure is usually governed by flexure and their strength is limited by
22 relatively low axial loads, failure is usually governed by flexure and their strength is limited by
23 rocking or crushing of the bricks. For stockier walls, shear behaviour usually dominates in the
24 rocking or crushing of the bricks. For stockier walls, shear behaviour usually dominates in the
25 form of shear sliding or diagonal cracking failure mode, either at the mortar joint interfaces or
26 form of shear sliding or diagonal cracking failure mode, either at the mortar joint interfaces or
27 through the brick units. Shear failures are characterised by more brittle behaviour, which can
28 through the brick units. Shear failures are characterised by more brittle behaviour, which can
29 lead to catastrophic collapses of buildings. In turn, damage in URM buildings during past
30 lead to catastrophic collapses of buildings. In turn, damage in URM buildings during past
31 earthquakes, often associated with brittle in-plane shear failure of masonry walls, has resulted
32 earthquakes, often associated with brittle in-plane shear failure of masonry walls, has resulted
33 in numerous casualties and severe economic losses [8]. Only in 2023, two high-magnitude
34 in numerous casualties and severe economic losses [8]. Only in 2023, two high-magnitude
35 earthquakes (Turkey-Syria and Marrakesh-Safi) devastated countries with large stocks of URM
36 earthquakes (Turkey-Syria and Marrakesh-Safi) devastated countries with large stocks of URM
37 buildings killing more than sixty thousand people and causing large-scale damage to
38 buildings killing more than sixty thousand people and causing large-scale damage to
39 households and infrastructure, with very high economic losses. In light of the above, finding an
40 households and infrastructure, with very high economic losses. In light of the above, finding an
41 effective seismic retrofitting solution, which will increase the deformability and thus the safety
42 effective seismic retrofitting solution, which will increase the deformability and thus the safety
43 of existing URM structures in seismic-prone areas is of fundamental importance.
44 of existing URM structures in seismic-prone areas is of fundamental importance.

45 To date, several different retrofitting systems designed to improve the in-plane behaviour of
46 To date, several different retrofitting systems designed to improve the in-plane behaviour of
47 URM masonry walls have been investigated experimentally. These include repairs with
48 URM masonry walls have been investigated experimentally. These include repairs with
49
50
51
52
53
54
55
56
57
58
59
60
61
62
63
64
65

external steel strips [9-10], steel reinforced concrete and ferrocement jackets [11-13], as well as externally bonded advanced composites such as fibre-reinforced polymers (FRP) [14-16] or textile-reinforced mortars [17-20]. These strengthening methods proved to be effective in improving the overall shear behaviour of walls; however, they are usually expensive, require a great deal of preparation time and affect the appearance of masonry, which in case of heritage structures is often unacceptable. Refined retrofitting methods, which provide more balanced options without changing the aesthetics of masonry include structural repointing interventions where steel [21-22] or FRP [23-26] reinforcement is mounted near to the surface of the wall (NSMR). This method can be particularly useful as it allows strengthened walls to perform akin to reinforced masonry (RM), and thus be designed using standard provisions for new RM structures. Such solutions can enhance the in-plane behaviour of masonry; however, these systems also have some limitations in relation to the installation and their performance. Due to the lack of flexibility in either regular steel bars or FRP bars, the installations can only be performed in the bed joints, and on regular masonry without affecting the appearance of the structure. In addition, these systems seem to improve the cracking behaviour primarily at low displacement demands, but show reduced performance at the stage of severe damage in masonry. In fact, with increasing horizontal displacement demands, the bond and the composite action between regular steel/FRP reinforcement and masonry degrades and in turn the ductility and energy dissipation capacity are limited. However, it is often the ductility that helps to prevent brittle collapse of the structure during strong earthquakes [27-28].

An alternative to FRP or regular steel bars can be stainless steel helical reinforcement, which is widely used as masonry connectors and reinforcement for various structural repairs of masonry. Alongside being used as wall ties or connectors, helical bars can be also installed as near-surface mounted reinforcements, fitted into slots cut into mortar joints, bonded using cement or polymer-based grout and finished with colour matching mortar. Being cold rolled from a plain round wire and subsequently tensioned through a free-twisting process, such reinforcement

1 offers high durability and superior mechanical properties when compared to alternatives due to
2 its increased strength and its helical shape, which offers additional mechanical interlock in the
3 masonry. As such, the helical shape of the bar ensures a desirable balance between flexibility,
4 strength, and bond, enabling reinforced masonry to reach larger deformability levels compared
5 to regular steel bars. Moreover, the flexibility of stainless-steel helical bars makes it possible to
6 bend them by hand and place them into both bed and head joints, and hence, the retrofitting can
7 be carried out without any major changes to the appearance of the masonry.
8

9
10 Although research on stainless steel helical bars is very limited, recent studies have indicated
11 that such reinforcement could be used for seismic retrofitting applications. Pull-out tests of
12 helical connectors from masonry substrates [29-30] generally showed good performance related
13 to bond strength, anchorage length, and mitigation of strength degradation during cyclic
14 loading, which highlights the potential for this reinforcement in seismic retrofitting
15 applications. Experimental investigations of helical bars in tension [31] revealed a good level
16 of ductility (extended the yielding plateau at ultimate load) and a minor effect of cycling on
17 strength. The effectiveness of helical reinforcement for shear strengthening of masonry walls
18 has been investigated experimentally [32] and numerically [33] on masonry wallets subjected
19 to diagonal tension; significant gains in shear strength and ductility were observed in the
20 retrofitted walls compared to URM walls. Recent research on the performance of masonry T-
21 connection joints [34] retrofitted with helical bars used as connectors subjected to cyclic out-
22 of-plane loads indicated that such reinforcement can significantly increase the energy
23 dissipation capacity.
24

25
26 Although initial test results on the performance of helical bars indicate that they can be used for
27 seismic retrofitting applications, to date this has not been experimentally verified in masonry
28 piers subjected to shear – critical structural members resisting earthquakes. The previous studies
29 [32, 33] involved monotonic loading of walls under diagonal compression without including
30
31
32
33
34
35
36
37
38
39
40
41
42
43
44
45
46
47
48
49
50
51
52
53
54
55
56
57
58
59
60
61
62
63
64
65

the effect of vertical stress and cyclic loading thus offering only limited information on the seismic performance.

The present study, for the first time investigates the use of helical bars for seismic retrofitting of URM masonry walls through full-scale tests on masonry walls subjected to cyclic quasistatic in-plane loads representing seismic actions. Moreover, some novel retrofitting patterns of helical bars are explored, in addition to ‘traditional’ ones involving repointing of bed joints. The results of this experimental study will contribute towards developing novel ductile retrofitting systems for URM walls in seismic prone areas, thus improving the safety of masonry buildings during earthquakes and increasing their resilience to seismic activities.

2. Experimental programme

The main testing programme comprised in-plane cyclic shear tests on cantilever masonry walls subjected to different levels of axial loading and retrofitted with various patterns of helical bars.

A total of nine tests were carried out: two on URM walls and seven on retrofitted walls using two levels of axial load. The different reinforcement patterns aimed to investigate the contribution of the reinforcement to the strength, ductility, and energy dissipation capacity of the masonry walls. In addition to reinforcement patterns used in previous studies, by taking advantage of the flexibility of the helical bars, a unique retrofitting configuration was explored where the reinforcement was placed into the mortar joints chasing bed joints and head joints without cutting through brick units (a “wiggled” pattern). One of the URM walls was tested under a low axial load, and after the testing, was repaired and re-tested to attest to the practical aspects of the application. The tests were complemented by material tests on masonry brick units, mortar, and grout samples as well as helical bars, to evaluate materials’ strength.

2.1. Wall specimens

All wall specimens were built as single-leaf masonry walls using solid fired clay masonry units laid in a running stretcher bond with a half brick overlap maintaining approximately 10 mm thick horizontal and vertical mortar joints (Fig. 1). The overall dimensions of the wall

specimens were 1115×975 mm resulting in an aspect ratio of 0.87. The nominal thickness of the wall was equal to the thickness of one brick, i.e. 102.5 mm. The walls were built onto adapters fabricated using parallel flange channels (PFC) with steel rebars welded inside and then infilled with concrete (40 MPa), with cast-in inner threads welded to the bottom of the PFC to enable a connection to the steel test frame. Prior to being infilled with concrete, a number of the adapters were fitted with helical bars, which would later form vertical reinforcement to the wall specimens to ensure good anchorage to the base.

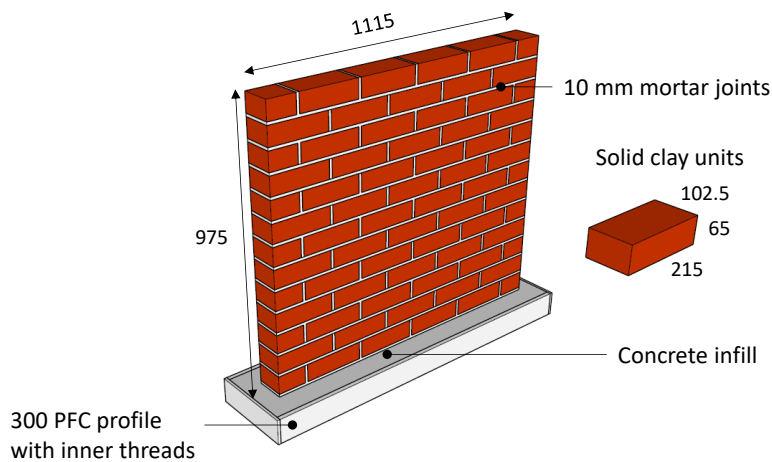


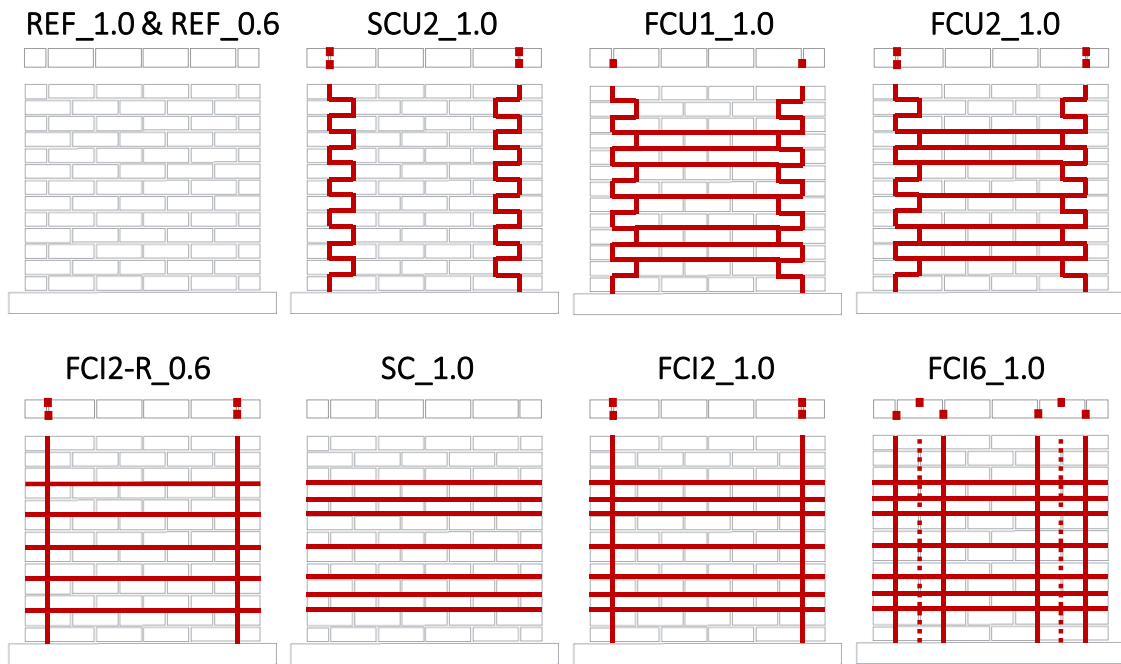
Fig. 1. Geometry of the wall specimens (dimensions in mm)

The properties of the wall specimens are listed in Table 1. Two levels of axial stress were investigated, equal to 0.6 MPa and 1.0 MPa. These stress levels correspond to about 7 % and 12 % of the masonry compressive strength and represent typical stress levels in low and medium rise masonry buildings, respectively [35]. One reference URM specimen and six retrofitted specimens were tested with an applied axial stress equal to 1.0 MPa, and two wall specimens (one URM and one retrofitted) were tested with an axial stress of 0.6 MPa. The two tests with the lower axial stress were carried out on the same specimen. Firstly, the URM wall was tested to failure and then it was retrofitted with helical bars and retested under the same axial stress of 0.6 MPa.

Table 1. Test specimens and retrofitting patterns.

	ID tag	Vertical load (MPa)	Vertical reinforcement		Horizontal reinforcement	
			type	no. per testing direction	type	no. per wall
1	URM 1.0	1.0	-	-	-	-
2	FCU1 1.0	1.0	wiggled	1	bed joint	7
3	FCU2 1.0	1.0	wiggled	2	bed joint	14
4	SC 1.0	1.0	-	0	bed joint	14
5	SCU2 1.0	1.0	wiggled	2	-	0
6	FCI2 1.0	1.0	straight	2	bed joint	14
7	FCI6 1.0	1.0	straight	6	bed joint	14
8	URM 0.6	0.6	-	-	-	-
9	FCI2-R 0.6	0.6	straight	2	bed joint	10

The reinforcement patterns for all walls are shown in Fig. 2. Three of the retrofitted specimens had “wiggled” helical bars (alternating in the horizontal and vertical direction in each course) as reinforcement, installed without cutting through the brick units, while three had vertical helical vertical bars installed into straight slots cut into the brick units. All retrofitted walls had helical bars placed into horizontal mortar joints in patterns as per Fig. 2. SC_1.0 and SCU2_1.0 had only one type of reinforcement (horizontal or vertical bars, respectively) to investigate the individual contribution of this reinforcement to overall capacity. FCU1_1.0 and FCU2_1.0 had the same reinforcement pattern (“wiggled” vertical bars and horizontal bars) with the latter having twice the amount of reinforcement to investigate how the reinforcement ratio affects the global response of the wall. FCI2_1.0 had the same pattern as FCU2_1.0, but straight bars were used instead of wiggled bars to investigate the difference in performance of these two reinforcement patterns. FCI6_1.0 had six helical bars installed vertically on both sides of the wall in a staggered pattern, representing walls with a high vertical reinforcement ratio.



*Note that all vertical bars were fitted into the PFC adapter prior casting concrete infill to achieve full anchorage in the base.

Fig. 2. Reinforcement patterns for all wall specimens.

2.2. Materials

The mechanical properties of the materials used to build and retrofit the walls were determined experimentally prior to the main testing programme. The experimental characteristics of the materials were then used to estimate the theoretical capacity of the walls. The material tests comprised compression tests on bricks and masonry prisms to determine the compressive strength and modulus of elasticity; bending tests on brick assemblages to determine the flexural strength of the bricks; compressive and flexural tests on the masonry mortar and grout; and tensile tests on helical bars to determine the mechanical properties of the reinforcement. Standardised shear tests on brick triplets were also carried out to estimate the initial shear strength and friction coefficient for the masonry joints.

2.2.1. Brick units

Standard solid clay masonry units were used in the present study with overall nominal dimensions of 102.5×215×65 mm (tolerance: length, ± 4 mm; width, ± 3 mm; height, ± 2 mm) and a nominal density of 1830 kg/m³. The compressive strength of the brick units was determined according to RILEM provisions [36]. The tests were performed on two sets of brick

units, with three units per set to account for the variability in the materials: (i) with the load applied normal to the brick headers; (ii) with the load applied normal to the beds. The loaded surfaces had a 5 mm gypsum capping to ensure that load will be distributed uniformly across the loading area. The average compressive strength was equal to 23.8 MPa (COV 9 %) for the direction normal to the headers and 28.9 MPa (COV 7 %) for the direction normal to the beds. The Young's modulus was measured during the compressive strength tests, where the units were tested in an upright (soldier) orientation, based on the readings of two LVDTs attached to the stretchers (Fig. 3). The base length of the gauges was set at 150 mm and a constant displacement rate of 0.2 mm/min was used. The elastic modulus was estimated between the stress levels corresponding to 30-60% of the failure stress as an average across the three specimens. The mean value of the experimental elastic modulus of the bricks was equal to 5691.1 MPa (COV 20%) with a maximum mean strain of 0.0039 (COV 6 %).



Fig. 3. Masonry unit tested under compression before and after failure.

The tensile properties of the masonry units were also estimated in line with RILEM provisions [36]. A typical specimen consisted of three bricks bonded together header-to-header using a very strong binder (with 1 day compression strength equal to 40 MPa), thus enforcing the failure in the masonry unit, under the loading point of a 3-point bending configuration over a 565 mm clear span (Fig. 4). The flexural tensile strength was determined from the tests as the maximum stress at failure and was equal to 1.43 MPa (COV 2 %).

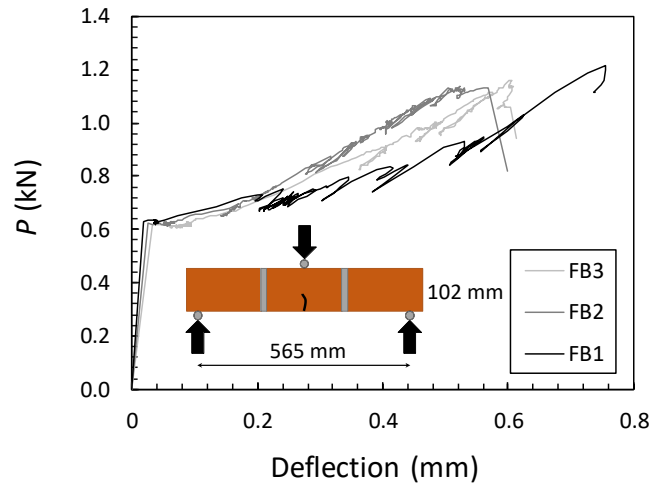


Fig. 4. Three-point bending test on brick-mortar assemblages.

2.2.2. Compressive strength of masonry and mortar

The mortar mix used to build the walls comprised cement-lime-sand composition with the ratio by volume equal to 1:2:8, respectively. The compressive and flexural strength of mortar was determined according to EN 1052-11 [37] on standard 40×40×160 mm prisms. The average values of compressive and flexural strengths were 5.1 MPa (COV 3 %) and 1.1 MPa (COV 6 %), respectively.

The compressive strength (perpendicular to the bed joints) and elastic modulus of masonry units were estimated according to EN 1052-1 [38] on four identical brick and mortar assemblages tested at a displacement rate of 0.2 mm/s. The stress-strain responses for all four specimens are shown in Fig. 5. The tests revealed an average compressive strength of 8.6 MPa (COV 5%) with a corresponding peak strain of 0.0068 (COV 11%). The average experimental modulus of elasticity was estimated as 1772.1 MPa (COV 8 %).

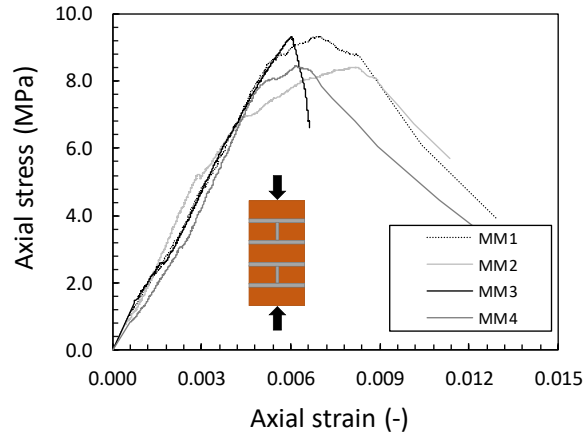


Fig. 5. Compressive characteristics of masonry brick-mortar assemblages.

2.2.3. Initial shear strength

The initial shear strength and the coefficient of friction were estimated according to EN 1052-3 [39] using the test setup shown in Fig. 6. The shear stress was determined at three different precompression levels, i.e. 0.2 MPa, 0.6 MPa, and 1.0 MPa. Three tests were carried out at each precompression level, totalling nine samples. The coefficient of friction was estimated as 0.6 and initial bond strength as 0.59 MPa.

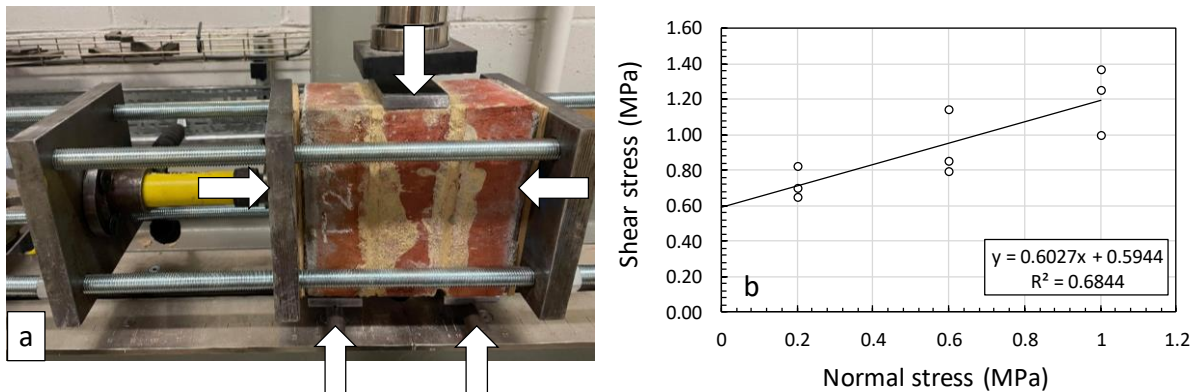


Fig. 6. Initial shear strength – test rig and results: a) test rig; b) test results for all 9 triplets

2.2.4. Helical bars and grout

The retrofitting system consisted of helical bar with an overall diameter of 6 mm (Fig. 7) and a cement-based pumpable and thixotropic bonding agent (grout). The shape of the helical bar offers great flexibility, thus allowing for easy bending and installation in masonry joints. The mechanical properties of the helical bars were determined with standard tensile tests on three bar samples using the provisions set out in ISO 6892 [40].



Fig. 7. Geometry of the helical bars

Strain was measured using an external extensometer with a base length of 100 mm, spanning the centre of the sample. Due to the specific helical shape of the bars, direct tensile tests could not be performed without risking damage to the helical fins near to the grip jaws of the machine. Therefore, the bar ends were anchored within aluminium tubes of 10 mm internal diameter and filled with resin grout, which enabled a larger surface area of the helix to be gripped. In turn, all tested samples exhibited a rupture within the extensometer's measuring range, which is the intended failure mode for this test. The test setup and the stress-strain response for all three samples is shown in Fig. 8. The average tensile load measured during the test was 9.8 kN (COV 1 %); with a cross-sectional area equal to 8.3 mm², such load resulted in an average stress of 1180.7 MPa (COV 1%). Based on the test results, it was determined that the response of the helical bar was close to elastic up to a stress level of about 455 MPa, which seems to agree with the estimates from other tests on helical bars [29-30]. The results indicated that such reinforcement reaches higher stress levels at larger displacements and does not exhibit clear yielding point as in the case of mild steel reinforcement; hence, the 0.2 % proof stress value was also determined, which for three tests revealed a mean value of 917.8 MPa (COV 7%). The Young's modulus of the helical bars was estimated as secant modulus at the stress level corresponding to the elastic range (455 MPa, see Fig. 8b) was equal to 110.8 GPa (COV 9%). As can be seen, the elastic modulus is much lower than the modulus of normal steel but at the same time much greater stress levels can be attained in comparison to mild steel reinforcement. The cement-based grout, which is an integral part of this retrofitting system was tested using the same provisions as for the masonry mortar. The mean compressive and flexural strengths

after 28 days of curing were equal to 40.4 MPa (COV 4 %) and 4.1 MPa (COV 11%), respectively.

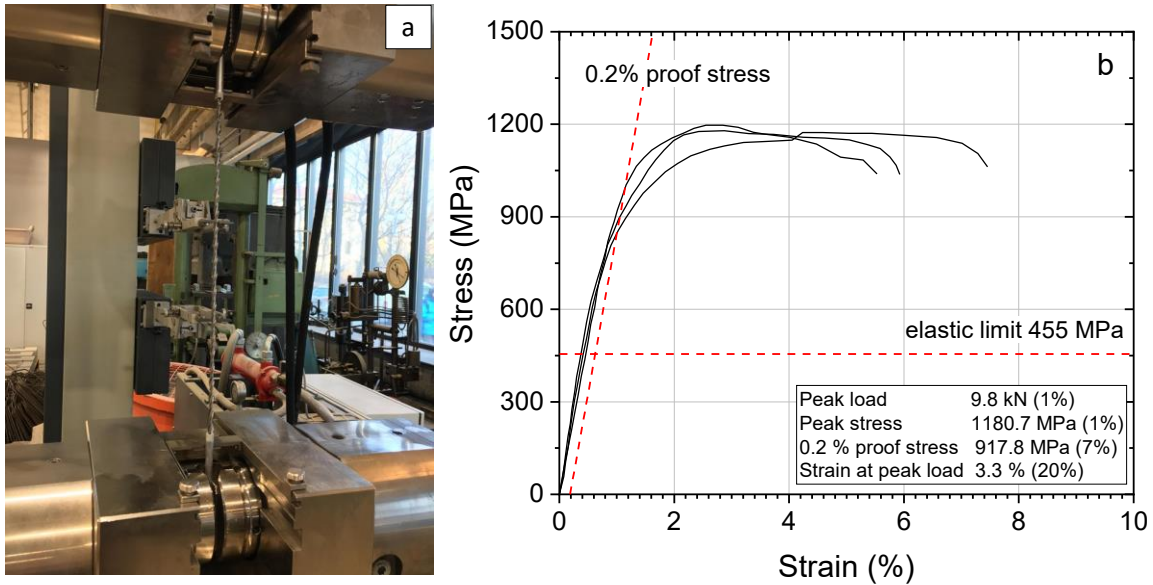


Fig. 8. Tensile testing: a) test setup; b) stress-strain response

2.3. Retrofitting with helical bars

The retrofitting was carried out on the masonry walls after a minimum of 6 weeks of curing at room temperature. All walls were retrofitted with the helical bars from the same batch with the same diameter of 6 mm. The following procedure was applied to carry out the installation:

- The existing mortar was raked out to a depth of approximately 25 mm, and then the slot was cleaned using compressed air and water. Straight slots were cut into both the mortar joints and masonry units for the specimens requiring straight vertical reinforcements.
- Helical bars were bent where necessary and cut to length to suit the slot.
- After ensuring that the cut slots were free from dust and debris, and were dampened, the grout was pumped into the back of the slot to fill approximately half of the depth. The procedure was carried out separately for vertical reinforcement and bed joint reinforcement.
- The vertical reinforcements were pressed into the grout first, followed by the bed joint reinforcements with the latter anchoring to the vertical reinforcement (Fig. 9).

- The final layer of grout was applied, providing about 15mm of cover to the helical bars.

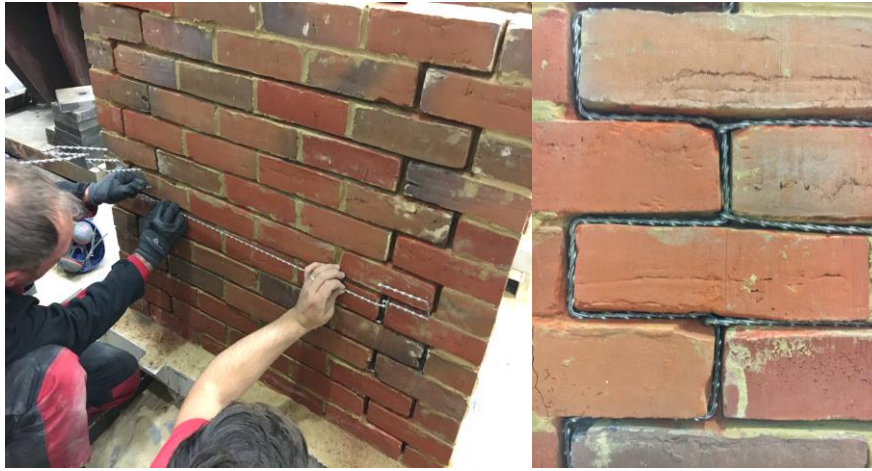


Fig. 9. Retrofitted helical bars, wiggled to both bed joints and head joints.

2.4. Test setup and methodology

The test setup used for all in-plane cyclic shear tests is shown in Fig. 10. All walls were tested as cantilevers, representing the lower half of a typical pier with an aspect ratio of around 1.75 fixed between the openings [41]. The bottom (300 mm PFC profile at the base of each specimen) was connected to the self-reacting test frame via 12 M24 bolts, thus being constrained against any displacement or rotation. The horizontal load was applied via a crosshead beam, which was free to rotate and translate in the in-plane direction. The bottom of the crosshead was filled with concrete and bonded to the top of the masonry wall using high strength grout, hence ensuring a strong bond between the two elements. The horizontal load was applied through two synchronised pin-ended hydraulic actuators, each with a nominal capacity of 100 kN. The vertical load was applied via a similar hydraulic pin-ended actuator, maintaining the design stress level. Additional in-plane guides were provided to ensure that any out-of-plane movements of the wall during the tests are prevented.

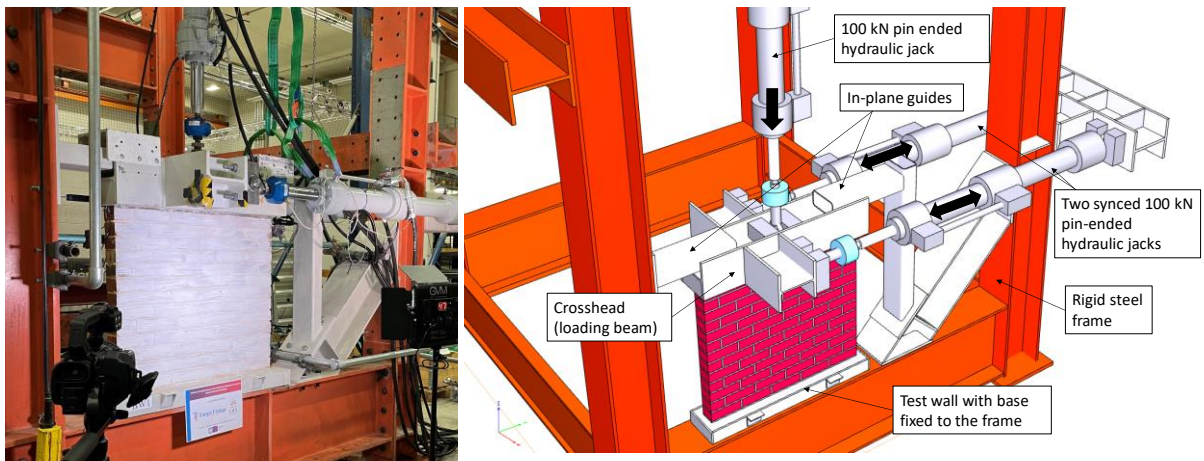


Fig. 10. Typical test setup for in-plane testing with cyclic reversals.

The experimental load was measured by two load cells built into the actuators; the horizontal shear capacity was taken as the sum of the loads recorded by the two horizontal actuators. The external instrumentation is shown in Fig 11. The net displacement of the wall was measured by an LVDT (P1) placed on top of the wall. Uplift was measured by LVDTs P2-P3, and the shear deformations were measured by wire gauges P4-P5.

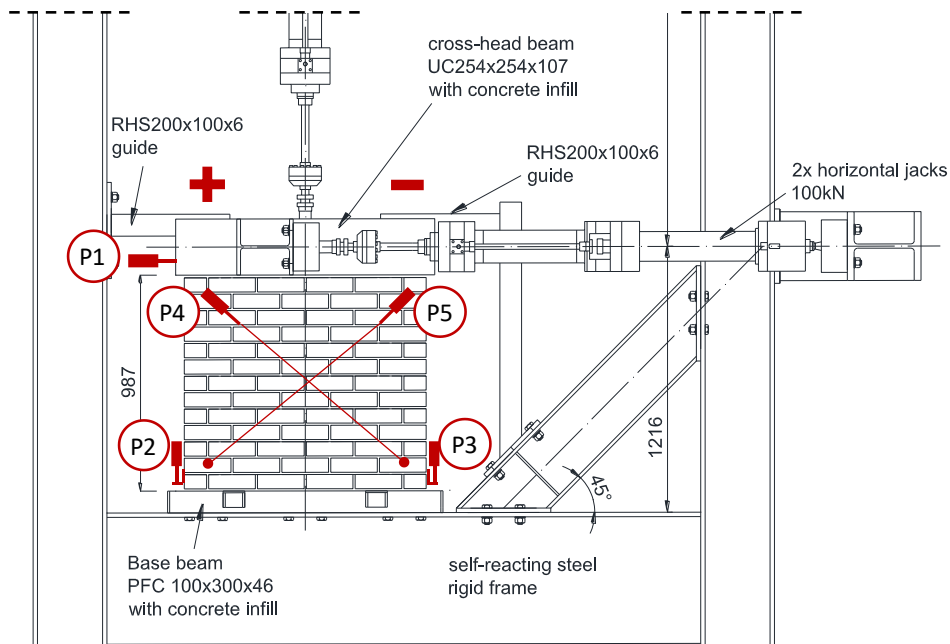


Fig. 11. Test setup and instrumentation – frontal elevation. Note that diagonal gauges were installed on the back side of the wall. The signs “+” and “-“ indicate directions of loading – push and pull, respectively.

The in-plane loading was applied in displacement control under quasi-static conditions to capture the post-peak softening stage and associated damage accumulation. The vertical stress was applied with a load-controlled regime. All wall specimens were subjected to the same in-plane reverse cyclic loading history shown in Fig. 12. The first two cycles were performed at target displacements of ± 0.25 and ± 0.50 mm to capture the elastic response of the wall specimen, while the subsequent cycles were performed at increasing target displacement amplitudes of ± 1 mm. The tests were terminated once a strength degradation of about 25% was observed, which is close to the level at which the element was considered to have reached its near-collapse limit state [42].

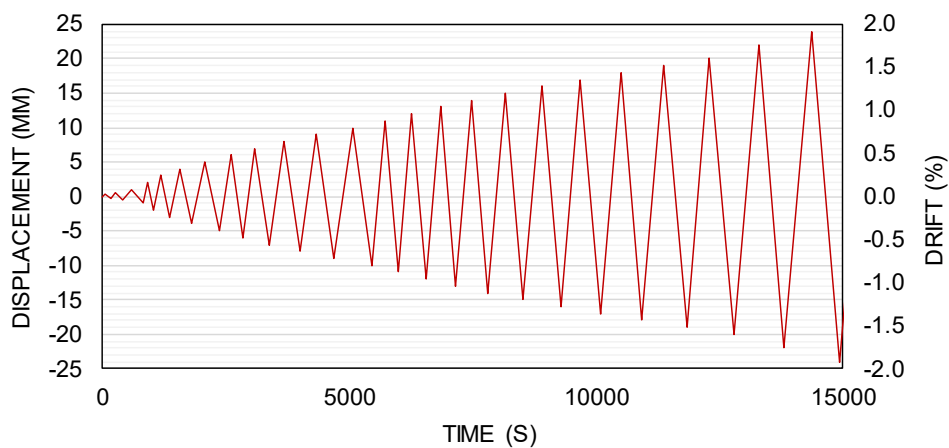


Fig. 12. Loading protocol adopted for the in-plane cyclic shear testing.

3. Test results and discussion

The main results for “push” (+) and “pull” (-) directions are summarised in Table 2. The reported values include the experimental horizontal shear capacity, V_{max} , taken as the sum of the loads measured by the two horizontal actuators and the experimental drift levels (computed based on the P1 readings), $\delta_{V_{max}}$ and δ_{max} , representing the drift of the wall at the peak horizontal load and the maximum recorded drift (corresponding to about 25 % load drop), respectively. The reported displacement values represent readings from LVDT P1, measuring the net displacement of the specimen.

Table 2. Main results of the in-plane cyclic shear tests

ID tag	σ_n (MPa)	V_{max} (kN)		$\delta_{V_{max}}$ (%)		δ_{max} (%)	
		Push	Pull	Push	Pull	Push	Pull
URM_1.0	1.0	+68.5	-69.4	+0.76	-0.67	+0.98	-0.88
FCU1_1.0	1.0	+65.3	-67.2	+0.80	-0.70	+1.87	-1.69
FCU2_1.0	1.0	+69.6	-69.1	+0.95	-0.82	+1.42	-1.39
SC_1.0	1.0	+66.5	-67.0	+0.67	-0.59	+1.05	-0.97
SCU2_1.0	1.0	+69.8	-71.1	+0.92	0.97	+1.59	-1.52
FCI2_1.0	1.0	+70.0	-67.5	+0.50	-0.54	+1.27	-1.25
FCI6_1.0	1.0	+68.5	-73.5	+0.50	-0.60	+0.95	-1.03
URM_0.6	0.6	+42.8	-45.1	+0.95	-0.90	+1.26	-1.00
FCI2-R_0.6	0.6	+45.8	-43.7	+0.79	-0.71	+1.75	-1.84

3.1. Failure modes and hysteretic response

The failure modes and cyclic in-plane responses for all walls are shown in Fig. 13 and Fig 14. Owing to their nature, the URM cantilever walls developed mixed failure modes involving various degrees of flexural and shear damage. Both URM walls initially developed flexural cracks in the horizontal mortar bed joint at the bottom of the wall, which kept opening until shear cracks started to appear and eventually led to brittle shear failure. The walls with near-surface mounted helical reinforcement developed different cracking behaviour, and, in turn, brittle shear failure was avoided, thus allowing for a more limited degradation of the in-plane load compared to the URM specimen. Although the natural variability of masonry led to some differences in the failure patterns on the left and right sides of the wall, a fairly symmetrical in-plane cyclic behaviour has been recorded up to the peak load capturing similar values of shear capacity and drift for both push and pull directions (Table 2). The difference between the maximum shear capacities recorded in the two loading directions was not more than about 7 % (5 kN, FCI6_1.0) whereas the difference across the drifts $\delta_{V_{max}}$ was about 16 % (0.13 %, FCU2_1.0). After reaching the peak load, and due to the different level of damage in the masonry per loading direction, the difference in the maximum drift values δ_{max} became more significant; up to 28 % (0.26%, URM_0.6).

Overall, the hysteretic response of the walls was characterised by a linear behaviour until the first cracks appeared at the base of the wall, followed by a progressive deterioration of lateral stiffness, indicating involvement of the mechanisms of rigid body motion (such as rocking of

the pier). The cyclical response of the walls retrofitted with helical bars did not show any major increase in the in-plane strength; however, the walls exhibited a different post peak response and some of the reinforcing patterns offered a more controlled failure mode and led to a larger displacement capacity. The next sections offer a more in-depth analysis of the results describing the failure mechanisms and hysteretic responses of each wall separately. It will be shown that certain combinations of helical bars can not only change the failure mode from brittle to ductile but can also lead to larger energy dissipation compared to a URM counterpart wall.

3.1.1. Test wall URM_1.0

The first cracks initiated in the mortar joint at the base of the wall at the interface between the masonry and the footing at a drift level of about 0.15 %. With increasing lateral load, the cracks propagated from the edges towards the centre of the wall until they formed one crack across the full length of the wall. This was associated with increased rocking of the wall and progressive degradation of the in-plane stiffness in the hysteretic load vs. drift response (Fig. 14a). Just before reaching the peak shear load, two shear cracks appeared (Fig 13a). The first crack occurred in the “push” direction and was shallow reaching only above the third course and represented the peak shear load. In the following cycle, in the pull direction, a steeper shear cracked formed, which was associated with a sudden drop in the stiffness and large in-plane displacement (Fig. 13a). Both cracks occurred at the masonry mortar interface with some cracks developing through the brick units, in the vicinity of the corners of the wall. The peak shear force attained by URM_1.0 was +68.5/-69.4 kN with the corresponding drift of +0.76/-0.67 %.

3.1.2. Test wall FCU1_1.0

After the first loading cycles, horizontal cracks started to develop along the interface with the concrete adapter at a drift of about 0.1 %, just slightly less than it was observed for the unreinforced counterpart indicating a minor contribution to the in-plane stiffness at the early stages of loading. However, the vertical portion of the “wiggled” reinforcements between the concrete base and the first course effectively bridged the crack, which led to the redistribution

of the loads and some horizontal cracks appeared between the first and the second course from the bottom bed joint where wiggled bars were chased into the bed joints (Fig 13b). As the loading progressed, the width of the crack further increased, which eventually led to compression crushing at the bottom corner bricks of the wall. These cracks coincide with reaching the maximum capacity of the specimen +65.3/-67.2 kN and the subsequent onset of strength loss. The wall did not lose strength rapidly with increasing displacement but exhibited an ability to maintain a residual strength capacity of about 75 % for the pull and 67 % for the push directions, at a large drift of +1.87/-1.69 %. It is evident that the two “wiggled” bars installed into the joints, combined with bed joint bars, somewhat contributed to the wall’s structural response; although not being able to increase the lateral load capacity of the wall, still managed to provide a better controlled post peak strength degradation and prevented shear cracking and a brittle collapse.

3.1.3. Test wall FCU2_1.0

The second wall with an increased number of the “wiggled” bars showed similar initial response to its counterpart wall FCU1_1.0. As in the previous test, the cracks developed at the second from bottom course, but overall, more damage was present after the onset of cracking and as the load progressed (Fig 13c, Fig. 14c). The beneficial effect of the increased reinforcement ratio on the global response of the wall was a higher drift capacity at peak load, equal to +0.95/-0.82 %, as well as the increased area of hysteresis loops, manifesting an increased energy dissipation capacity. On the other hand, the larger drifts resulted in increased compression in the toe regions of the wall and hence caused more damage to the brick units compared to its counterpart wall FCU1_1.0, and the result was that a non-symmetric post-peak response was achieved with failure in the push direction, where significant toe crushing developed.

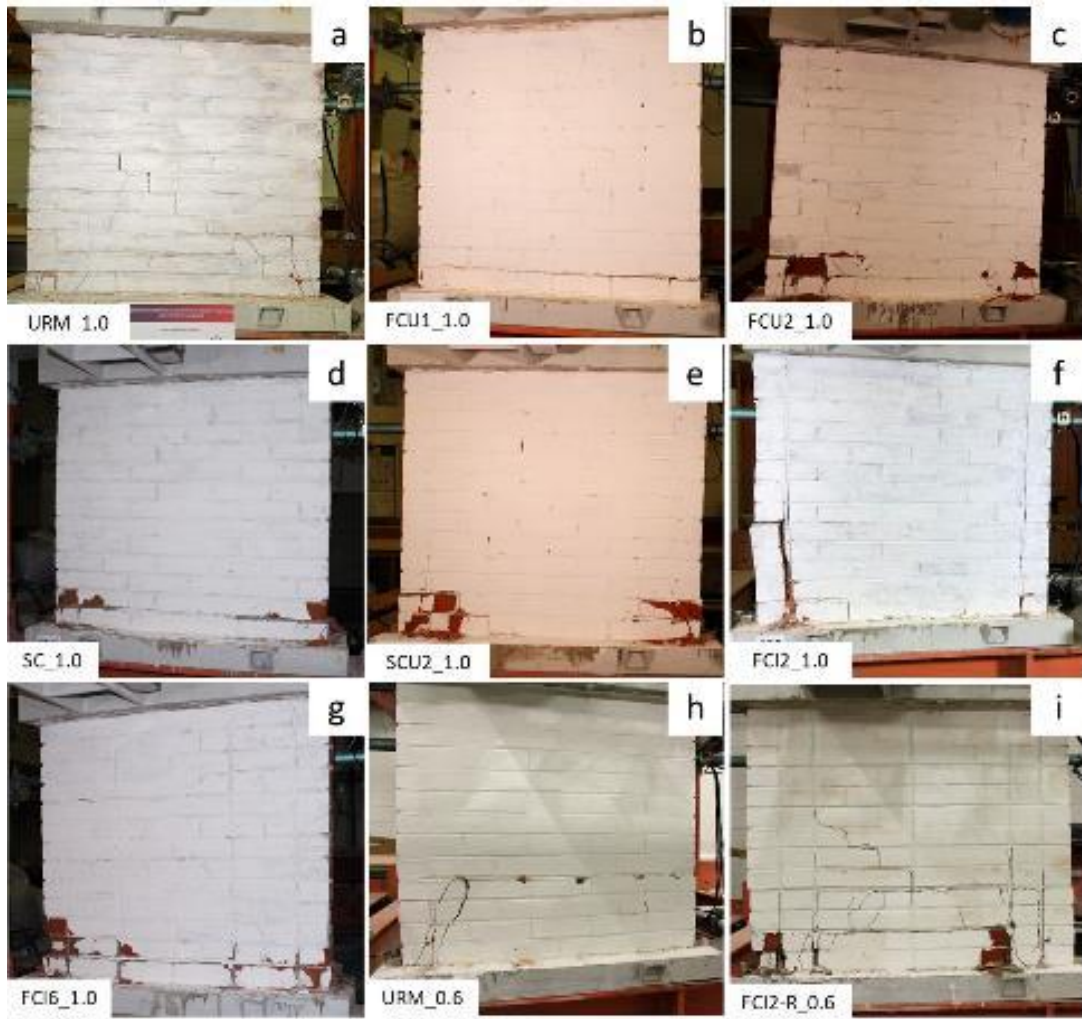


Fig. 13. Failure patterns for all walls.

1
2
3
4
5
6
7
8
9
10
11
12
13
14
15
16
17
18
19
20
21
22
23
24
25
26
27
28
29
30
31
32
33
34
35
36
37
38
39
40
41
42
43
44
45
46
47
48
49
50
51
52
53
54
55
56
57
58
59
60
61
62
63
64
65

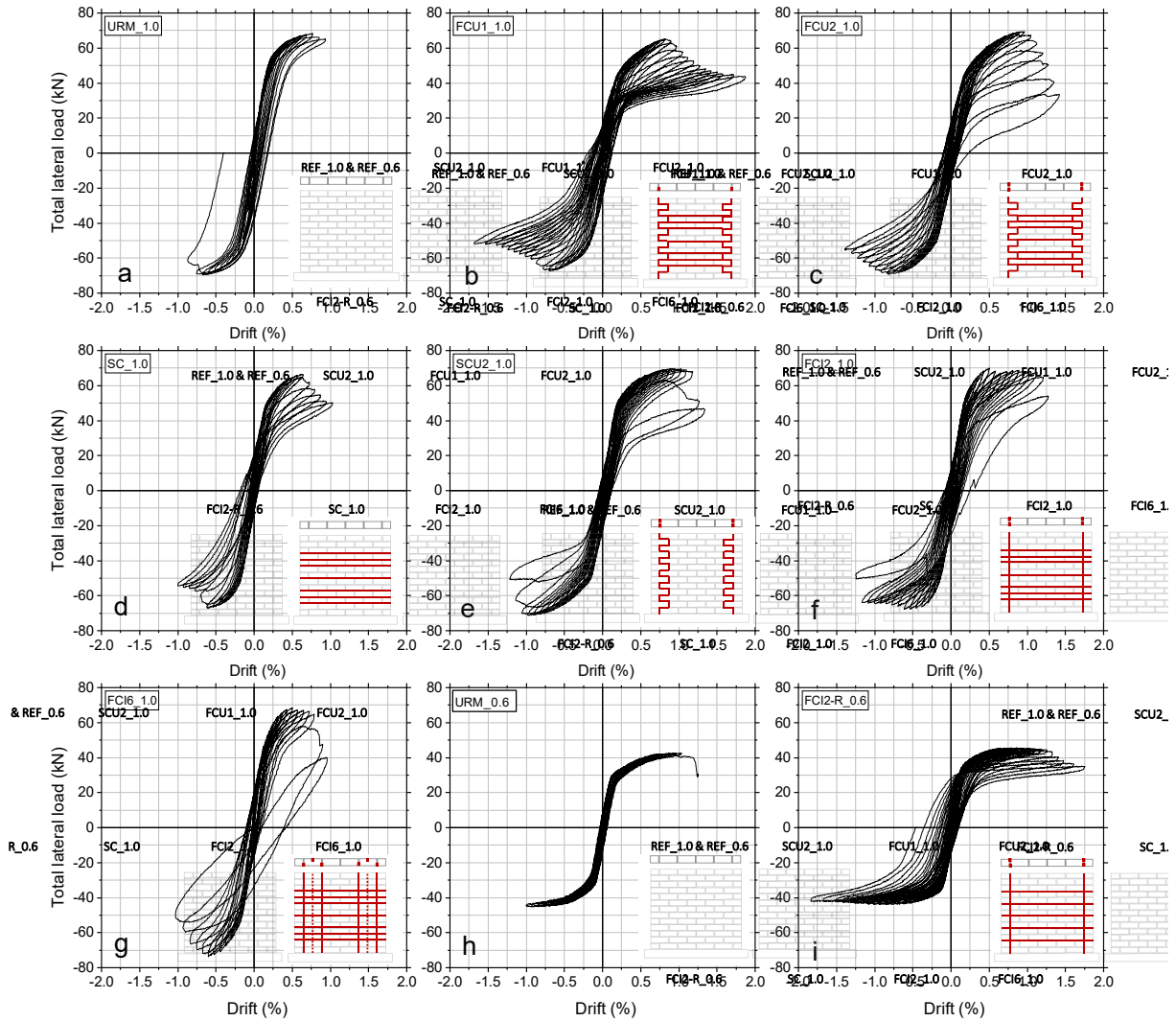


Fig. 14. Load-drift hysteresis loops for all walls.

3.1.4. Test wall SC_1.0

The wall retrofitted only with bed joint reinforcement showed at initial stages a behaviour similar to the corresponding URM wall, but this behaviour changed with increasing displacement demands and a more ductile response was achieved at the ultimate stage and beyond the peak. The first cracks developed in the push direction (Fig. 13d) in the second from bottom course at about 0.15 % drift – the same drift level as in the case of URM_1.0. At the peak load of +66.5/-67.0 kN, a drift of +0.66/-0.59 % was attained exhibiting almost the same load path as the URM wall. However, after reaching the maximum load, shear cracks did not occur but failure was induced in the toe regions leading to a compression failure of the two

1 bottommost corner bricks. This manifested on the hysteretic response as a sudden load drop at
2 the end of the cycle, and triggered a progressive loss of strength. With further increase of the
3 load, it stabilised, maintaining more than 75 % of the peak lateral capacity before the test was
4 terminated. Although strength of the wall did not increase (indicating that lateral load capacity
5 was governed by flexure/rocking rather than by shear strength) the use of bed joint bars alone
6 allowed to avoid shear cracking and enabled a more controlled failure of the wall.
7

13 3.1.5. Test wall SCU2_1.0

14 As expected, at a drift level of 0.15 % cracking developed in the bed joint, which was not
15 reinforced as in FCU2_1.0, however, as the displacement increased, the cracks did not progress
16 from both sides as in the case of FCU2_1.0. Although “wiggled” reinforcement has been
17 somewhat engaged, and even slightly increased the wall’s capacity reaching a peak of +69.8/
18 71.1 kN was recorded, the high demand put on the vertical wiggled bars led to separation of the
19 two toes from the wall just below the third course where the bar had its second bend (Fig. 13e).
20 This caused a rapid loss of strength and led to a global failure of the wall without any capacity
21 to preserve residual strength. Although the presence of the “wiggled” reinforcement (as
22 expected) did not lead to higher lateral load capacity, it improved the hysteretic energy
23 dissipation, albeit not to the extent that it did in the specimen (FCU2_1.0) with a combination
24 of “wiggled” and horizontal bars.
25

42 3.1.6. Test walls FCI2_1.0 and FCI6_1.0

43 The wall specimens with straight vertical reinforcement installed into slots cut through the
44 bricks and the mortar head joints recorded comparable performance levels to the walls with
45 “wiggled” bars up to the peak load, however, they showed limited capability to control the
46 failure of the wall. FCI2_1.0 cracked at a drift of 0.12% at slightly higher load level than the
47 URM wall. It is noted that although vertical bars were anchored into the footing, the wall did
48 not seem to behave as a proper reinforced masonry wall, with increase in lateral load capacity
49 proportional to the vertical reinforcement added. The wall developed a slightly stiffer response
50
51
52
53
54
55
56
57
58
59
60
61
62
63
64
65

1 compared to the URM members in the push direction, and almost an identical load path in the
2 pull direction. At a drift of about 0.5 %, cracks along the vertical reinforcement appeared and
3 this effectively stopped the load from further increasing. Despite this, the wall maintained most
4 of its capacity until reaching a drift of about 1.1-1.2 % when a large part of the masonry
5 separated from the wall (Fig. 12f) and triggered the failure. In an attempt to avoid such a failure,
6 the wall FCI6_1.0 had installed more straight bars installed in a staggered pattern (front/rear,
7 see Fig. 2), hence having the vertical reinforcement closer to the centre of the wall specimen.
8 The wall cracked at a low drift level of about 0.1 %, indicating a stiff response. Separation of
9 the masonry cover was avoided but having more flexural reinforcement led to similar lateral
10 load and displacement capacities and eventually a more brittle post peak degradation (Fig. 12g).

22 3.1.7. Test walls URM_0.6 and FCI2-R_0.6

23 The test on the second URM wall with a lower axial stress of 0.6 MPa showed a different failure
24 mode compared to URM_1.0. Initial cracks were observed at a drift of 0.1 % in the horizontal
25 bottommost mortar joint, and with increasing amplitudes these cracks propagated through the
26 bed joint and connected to form one continuous crack about which the wall rocked. The wall
27 rocked in-plane showing nonlinear elastic behaviour and no loss of strength without any signs
28 of sliding or crushing until reaching a drift of about 0.75 %. Just before reaching the peak load
29 in the pull direction, a diagonal crack formed on the left side of the pier, and, with increasing
30 displacement, the crack changed to horizontal above the fourth course (Fig. 13h), which
31 propagated through the entire bed joint ultimately leading to a sliding shear failure.
32
33
34
35
36
37
38
39
40
41
42
43
44
45
46

47 After the test, any damaged bricks were replaced, and the wall was retrofitted “as it stands”
48 using straight vertical and horizontal helical bars (see reinforcement patterns in Fig. 2). The
49 grout was allowed approximately 28 days to cure at room temperature, and then the same wall
50 was then tested as FCI2-R_0.6. Since some of the damage was already accumulated in the wall,
51 the initial stiffness did not increase significantly; the old cracks opened, and some new cracks
52 developed at a drift level of 0.15 % in both loading directions. The horizontal crack appeared
53
54
55
56
57
58
59
60
61
62
63
64
65

again; however, sliding was effectively resisted by the vertical bars resulting in an enhanced rocking capacity and much greater energy dissipation. The in-plane capacity was reached when toe-crushing failure was observed; however, the strength decay was gradual and smooth enabling reaching a 20 % strength loss at +1.75/-1.84 % drift level despite a shear stepped crack developing in the pull direction Fig 13i, Fig.14i).

3.2. In-plane stiffness

The experimental secant stiffness was estimated as the ratio of the total lateral force per direction to the corresponding displacement amplitude. All retrofitted walls exhibited a similar degradation of lateral stiffness, hence, only four specimens are shown for brevity (URM and three RM specimens, Fig. 15). As can be seen, the addition of helical reinforcement somewhat increased the initial in-plane stiffness; however, it did not substantially change the post-cracking stiffness compared to URM_1.0 wall regardless of the retrofitting pattern, and both the “wiggled” and the straight flexural bars yielded a similar response. Although stiffness did not increase, the helical bars allowed for extending the stiffness degradation path and enabled larger drift levels to be achieved.

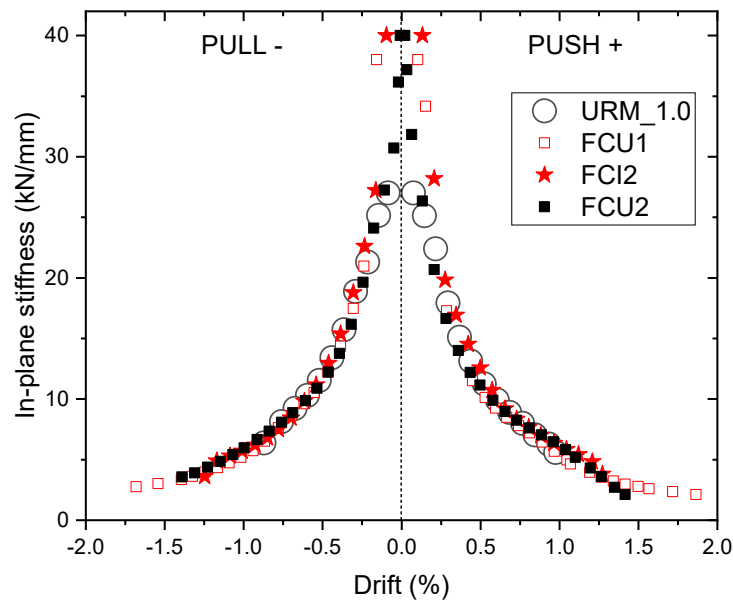


Fig. 15. Typical degradation of in-plane stiffness.

3.3. Definition of yield displacement and ductility factor

Owing to their inherent heterogeneity and low deformability, masonry members are characterised by nonlinear response and lack of a clear yielding point, thus making it difficult to distinguish elastic and plastic stages of the structural response. Various mathematical simplifications were proposed and introduced into design codes to simplify the analysis and idealise the real response using linear approximations, assuming elastic, homogenous and isotropic global properties of masonry. Current design procedures for masonry members often recommend using a bilinear elasto-plastic idealisation, which is deemed capable of adequately representing the simplified response of masonry [6, 43-44]. The bilinear force-displacement relationships (a typical one is shown in Fig. 16) were obtained from experimental envelopes, using average values of initial stiffness and ultimate post-peak displacement Δ_{max} corresponding to about a 25 % loss of strength. Knowing the two mentioned values, the ultimate resistance V_{ult} can be computed as:

$$V_{ult} = K_e \left(\Delta_{max} - \sqrt{\Delta_{max}^2 - \frac{2A_{env}}{K_e}} \right) \quad (1)$$

The elastic stiffness K_e was determined based on experimental data and was taken as a ratio between the measured experimental lateral load at onset of cracking, V_{cr} , and the corresponding displacement at cracking, Δ_{cr} . The value A_{env} is the average area under the experimental envelope curves and represents the total energy dissipated during the test per direction. The shape of the idealised bilinear response (red curve in Fig. 16) was determined by imposing that the total energy of the experimental response is equal to the total energy of the bilinear response. The experimental and idealised characteristics of the in-plane responses are listed in Table 3. The values obtained from this analysis seem to be consistent with the literature and close to current design recommendations. The average experimental crack limit was $0.69V_{max}$ (COV 12 %), which is in very good agreement with the limit proposed by Tomažević [6] ($0.70V_{max}$) and is less conservative than the 40% to 60 % crack limit provisions proposed in key design codes

(EC8 [43], FEMA [44], ASTM [45]). The ratio between the idealised and experimental maximum shear resistance V_{ult}/V_{max} oscillated around 0.9 (0.89, COV 6 %), which is in line with the findings of previous studies ([5-6], [12],[46]) and thus attests the validity of the analysis.

The idealised values of the yield displacement, Δ_{el} , and the displacement corresponding to the 25 % lateral load drop, Δ_{ult} , were used to assess the ability of the tested walls to withstand post elastic deformations. Key structural factors, such as global ductility factors (μ) and behaviour factors (q) were computed as:

$$\mu = \frac{\Delta_{ult}}{\Delta_{el}} \quad (2)$$

$$q = \sqrt{2\mu - 1} \quad (3)$$

Eq. 3 assumes that the fundamental period of the masonry building is in the equal energy region of the response spectrum. The computed values demonstrate significant improvements in post-peak behaviour (Table 3). For the URM wall, with larger vertical stress, the force reduction factor was equal to 2.6, which is close to the upper limit for URM walls in accordance with Eurocode 8. For most of the retrofitted walls the value of q factors exceeded 4.0, which represents a reduction factor greater than that proposed for reinforced masonry 2.5-3.0, thus indicating that large gains in ductility have been achieved. Both the test and re-test of the wall with lower stress level exhibited q factor larger than 4.0 with factors for the re-test equal to 4.5.

Table 3. Parameters of the idealised elastic and post-elastic behavior; ductility factor and behavior factor.

ID tag	$K_{el,exp}$ (kN/mm)	V_{ult} (kN)	V_{ult}/V_{max}	crack limit	Δ_{el} (mm)	Δ_{ult} (mm)	μ	q
URM_1.0	27	65.0	0.94	0.65 V_{max}	2.4	9.1	3.8	2.6
FCU1_1.0	38	57.9	0.88	0.60 V_{max}	1.5	14.1	9.3	4.2
FCU2_1.0	40	63.7	0.92	0.69 V_{max}	1.6	13.8	8.7	4.0
SC_1.0	28	61.8	0.93	0.71 V_{max}	2.2	8.6	3.9	2.6
SCU2_1.0	33	63.3	0.90	0.73 V_{max}	1.9	13.2	6.9	3.6
FCI2_1.0	45	63.6	0.92	0.85 V_{max}	1.4	13.3	9.4	4.2
FCI6_1.0	50	56.9	0.80	0.73 V_{max}	1.1	10.7	9.4	4.2
URM_0.6	25	34.7	0.79	0.68 V_{max}	1.4	11.9	8.6	4.0
FCI2-R_0.6	24	42.4	0.95	0.54 V_{max}	1.8	19.1	10.8	4.5

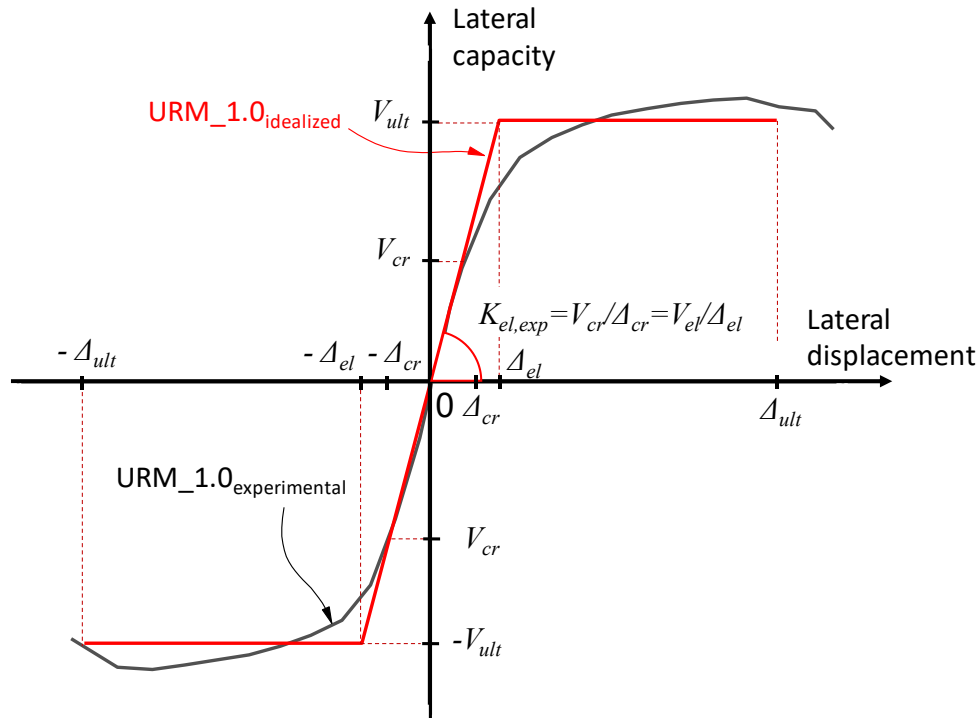


Fig. 16. Typical bilinear idealisation of force-displacement response.

3.3. Energy dissipation capacity

The cumulative energy dissipated during in-plane testing plotted against average drift in push and pull directions is illustrated in Fig 17. As can be seen, similar energy dissipation capacities were achieved for the walls with a larger axial stress up to drift levels of about 0.4 %, with the poorest energy characteristics exhibited by the URM_1.0 (Fig. 17a). However, as the drift levels increased, the walls with the straight vertical reinforcements (FCI2_1.0 and FCI6_1.0), as well as the wall lightly reinforced with “wiggled” reinforcement FCU1_1.0, showed improved energy dissipation performance compared to the URM wall. Compared to the latter, at a drift of 0.9 %, FCI6_1.0 dissipated about 50 % more energy and about 15 % more was dissipated by FCI2_1.0. At approximately the same drift level, FCU1_1.0 dissipated about 24 % more energy compared to the reference wall, and at ultimate showed the largest energy dissipation capacity. The remaining walls SC_1.0 and SCU2_1.0 showed similar, however, extended energy dissipation paths compared to URM_1.0, indicating that such retrofitting layouts might be less efficient during events like earthquakes, however, can still prolong the structure’s integrity. The

repaired and retested wall FCI2-R_0.6 showed more than a twofold increase in energy dissipation at ultimate than during the first test (Fig.17b). Based on the results it can be concluded that up to the maximum drift levels seen in URM, straight bars have a higher potential to dissipate energy than the wiggled bars, however both types of bars are able to prevent brittle collapse of the structure and are able to contribute to the total energy dissipation even beyond the peak lateral load. It is also worth noting that although a limited number of walls was tested, the bars turned out to be more effective in the elements axially loaded to 1.0 MPa and dissipated more energy than the walls loaded to 0.6 MPa.

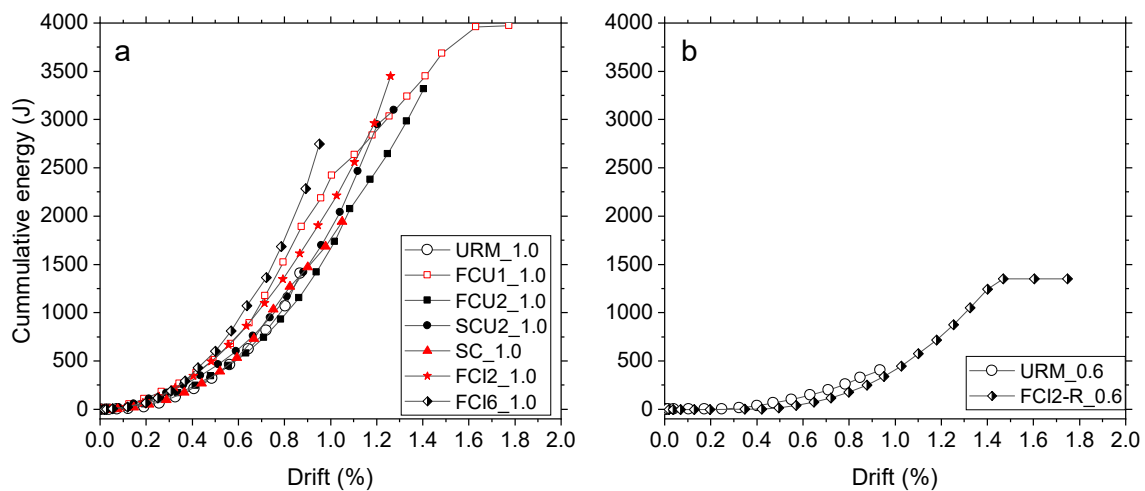


Fig. 17. Energy dissipation for increasing drift levels: a – walls specimens with an axial stress level of 1.0 MPa; b – walls with an axial stress level of 0.6 MPa.

4. Analytical predictions

The theoretical values of lateral load capacities associated with various failure modes (flexural, shear sliding, diagonal shear) were assessed using Eurocode 6 [47], which also has provisions for steel reinforcement, and hence can be used to estimate, by analogy, the contribution of helical bars to the total lateral load capacity. In the following sections, the contributions of the masonry and reinforcement were determined separately and were then compared with the experimentally derived peak load capacity. For comparing with test results, the safety factors were not taken into account in the code equations and the measured values of materials properties reported in section 2.2. were utilised.

4.1. Calculations for unreinforced masonry

4.1.1. Shear sliding

The model adopted in Eurocode 6 code is an extension of the Mohr-Coulomb criterion with an upper cap. The shear strength of unreinforced masonry is defined as the sum of the initial shear strength (shear bond at zero compression) and the contribution of the compressive stress perpendicular to the shear direction through friction. The characteristic shear strength of masonry at the critical section can be determined from:

$$\tau_{vk,1} = (\tau_{vk0} + \mu\sigma_d) \leq 0.065f_u \quad (4)$$

Where τ_{vk0} is the initial shear strength, μ is the coefficient of friction and σ_d is the design compressive stress. Eurocode 6 recommends $\mu = 0.4$, and, if no experimental data is available, τ_{vk0} can be assumed from tabulated values between 0.15 MPa and 0.3 MPa, or as recommended by the appropriate National Annex. The value of τ_{vk} is also limited to 6.5% of the compressive strength of the masonry unit, f_u , to avoid compression failure in the corners. The associated horizontal load (shear capacity) can be calculated as:

$$H_{sl} = t \cdot l_c \cdot \tau_{vk,1} \quad (5)$$

The experimental shear strength should be determined by taking into account only the length of the compressed part of the wall, neglecting the part in tension. The length l_c was calculated assuming linear distribution of compressive stresses (e.g. in [46]) resulting from the experimental loads. The value t represents the thickness of the wall. Verification of the experimental and theoretical shear capacities has been carried out using the material characteristics reported in section 2.2, using experimental values of τ_{vk0} and μ in lieu of the values recommended by Eurocode 6.

4.1.2. Diagonal cracking

The approach adopted in Eurocode 6 considers the shear strength of masonry as a main design parameter, and thus implicitly considers shear sliding as a failure mode that governs the global shear resistance of the members being designed. Although the procedure for estimating

diagonal cracking is not given in the main sections of the document, such provisions can be found in the National Annex DIN EN 1991 1-1/NA [48] and this criterion is based on Mann-Müller model [49]. According to the National Annex, the diagonal cracking strength can be estimated from:

$$\tau_{vk,2} = 0.45 f_{bt,cal} \sqrt{1 + \frac{\sigma_d}{f_{bt,cal}}} \quad (6)$$

Where $f_{bt,cal}$ represents the tensile strength of masonry units. The tensile strength of the units was not determined experimentally but derived from the flexural tests on masonry (see section 2.2.1). The tensile strength of brick units was calculated as the average reported flexural strength divided by 1.5, similar as in [50]. As such, $f_{bt,cal}$ was taken as $1.43\text{MPa}/1.5=0.9\text{MPa}$. As can be seen, this approach assumes that tensile strength governs shear behaviour of the walls and this model is a variation of the model established by Turnšek and Čačovič [51], which assumes that URM masonry behaves as an elastic, homogeneous and isotropic material.

The horizontal load associated with diagonal cracking strength was calculated as:

$$H_d = t \cdot l \cdot \tau_{vk,2} \quad (7)$$

4.1.3. Flexural resistance

The flexural resistance was determined based on force equilibrium. The bending moment was calculated as:

$$M_{Ru} = \frac{\sigma_d t L^2}{2} \left(1 - \frac{\sigma_d}{f_m} \right) \quad (8)$$

Where L is the length of the wall, t is the thickness of the wall and f_m is the experimental masonry strength. The lateral load corresponding to the flexural capacity was calculated as:

$$H_f = \frac{M_{Ru}}{h\alpha} \quad (9)$$

where h is the height of the wall and α is 1.0 (for cantilevers).

4.2. Calculations for reinforced masonry

4.2.1. Steel reinforcement contribution to shear resistance

According to Eurocode 6, the reinforcement contribution to shear capacity only comes from bed joint reinforcements, and can be calculated as:

$$H_{str,h} = 0.9A_{sh}f_{yh} \quad (10)$$

Where A_{sh} is the total cross-sectional area of horizontal reinforcement and f_{yh} is the allowable stress in the helical steel reinforcement. A_{sh} was assumed as the area of one helical bar (8.3 mm²) multiplied by the number of horizontal bars crossing the diagonal crack. Based on the tensile tests, the allowable stress in the helical bars was as the maximum stress at the elastic range, which was limited to 455 MPa (see Fig. 8).

4.2.1. Contribution to flexural resistance

The lateral flexural capacity was estimated using standard verification Eurocode procedure for reinforced concrete masonry members assuming rectangular stress distribution. The ultimate bending moment was computed as:

$$M_{Ru,v} = A_{sv}f_yz \leq 0.4f_m tL^2 \quad (11)$$

Where z is the lever arm of the internal forces. The area A_{sv} represented the total area of the vertical reinforcement installed on one side of the wall. The horizontal load associated with the moment was calculated as:

$$H_{str,v} = \frac{M_{Ru,v}}{h\alpha} \quad (12)$$

4.3. Summary of predictions and discussion

Results of the predictions are illustrated in Fig. 18, with the experimental-to-theoretical ratios listed in Table 4. Given that mixed failure modes were observed during testing, the contribution of bare masonry was verified against the models for flexural capacities and the two shear capacities (sliding/diagonal cracking) separately. The capacities of the wall specimens retrofitted with helical reinforcement were estimated as the sum of the contributions of unreinforced masonry and contribution of helical reinforcement. As such, for the flexure-controlled estimate, the total lateral in-plane capacity consisted of the flexural contribution of

the bare masonry wall (Eq. 9) and the contribution of the vertical helical bars (Eq. 12). The shear controlled-estimate comprised the component associated with shear resistance of bare masonry (either Eq. 5 or Eq. 7, depending on the failure mode observed during the experiment) and the contribution of the horizontal helical bars (Eq. 10).

Table 4. Predictions of lateral load capacity: experimental-to-theoretical ratios

ID tag	V_{max} (kN)	URM			RM	
		Sliding	Diagonal	Flexure	Shear-controlled*	Flexure-controlled
		$V_{max}/Eq.5$	$V_{max}/Eq.7$	$V_{max}/Eq.9$	$V_{max}/(Eq.7+Eq.10)$	$V_{max}/(Eq.9+Eq.12)$
URM_1.0	68.9	1.21	0.99	1.21	-	-
FCU1_1.0	66.2	-	-	-	0.71	1.09
FCU2_1.0	69.3	-	-	-	0.59	1.08
SC_1.0	66.7	-	-	-	0.57	1.17
SCU2_1.0	70.4	-	-	-	1.01	1.10
FCI2_1.0	68.7	-	-	-	0.58	1.07
FCI6_1.0	71.0	-	-	-	0.60	0.93
URM_0.6	43.9	1.29	0.71	1.23	-	-
FCI2-R_0.6	44.7	-	-	-	0.67	1.07

* for the walls with vertical stress 0.6 MPa for Eq.5 was used instead of Eq.7, as shear sliding was observed during the experiments.

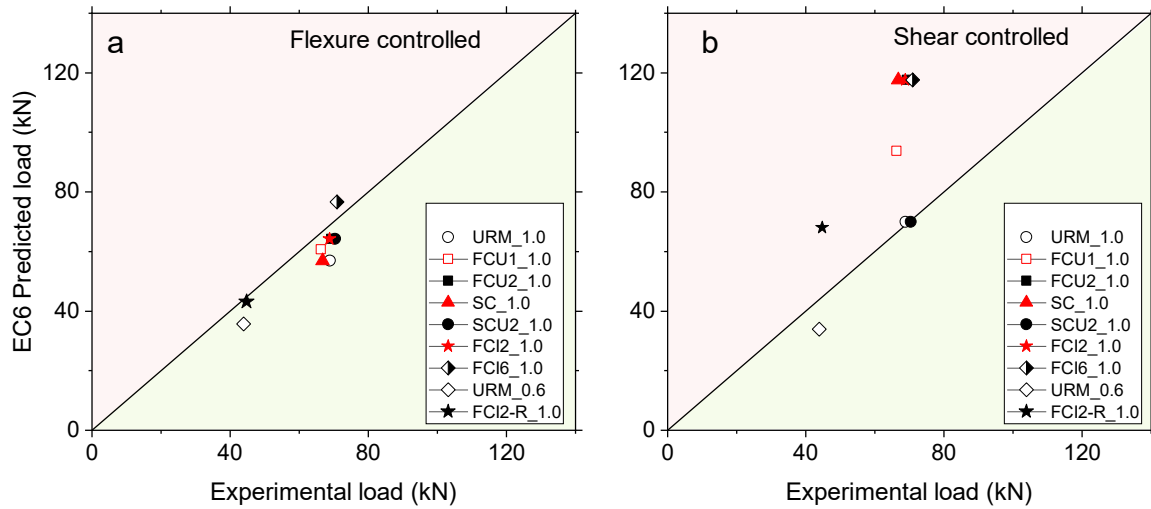


Fig. 18. Predictions of lateral load capacity: a – Predictions associated with flexural failure; b – predictions associated with shear failure.

4.3.1. Contribution of masonry

Based on the experimental observations on the URM walls, it is evident that both developed extensive flexural damage, which was followed by a shear failure. URM_1.0 failed due to

development of a diagonal stepped crack (whilst also exhibiting some cracks through the masonry units), whereas URM_0.6, after significant rocking, eventually failed due to shear sliding. It is worth noting that if rocking occurs first, there are no hardening mechanisms left, which can substantially increase the lateral capacity. Yet, the tests have shown that shear failures followed the rocking response, which indicates that shear resisting mechanisms have been already degraded due to cyclic loading, and hence, the initial shear resistance of the wall degraded too, and shear failure ensued. In turn, although both the URM walls exhibited shear failures, the initial flexural damage effectively limited the lateral in-plane capacity of the test walls, and thus, both checks (flexural and shear) should be carried out. As can be seen, flexural and shear predictions can give reasonable estimates of the in-plane lateral load capacity and confirm the experimental observations. For the failure modes corresponding to experimental observations, the predictions of shear resistance yielded ratios equal to 0.99 for diagonal cracking (URM_1.0) and 1.29 for shear sliding (URM_0.6). The prediction of flexural resistance yielded experimental-to-theoretical ratios equal to 1.21 and 1.23 for URM_1.0 and URM_0.6, respectively. Based on the predictions, it can be concluded that the theoretical shear capacities of the unreinforced cantilever walls were estimated reasonably well using Eurocode 6 provisions and the predictions are in a good agreement with the experimental behaviour.

4.3.2. Contribution of helical bars

As discussed before, helical bars prevented a brittle shear failure and led to the flexural failure associated with significant rocking and toe crushing. The flexure-controlled estimate, combining flexural contribution of bare masonry and the contribution of vertical reinforcement produced consistent and accurate predictions of the total lateral capacity, with average experimental-to-theoretical ratios equal to 1.07 (COV 8 %). It is also worth noting that almost all theoretical predictions (apart from FCI6_1.0, which was slightly overestimated) were on the safe side, even though safety factors were omitted in the calculations. On the other hand, if the walls were deemed shear-critical, and shear contribution of masonry is coupled with

1 contribution of the bed joint bars, the EC6 provisions led to overestimation of the total lateral
2 load capacity with average experimental-to theoretical ratios equal to 0.67 and large scatter in
3 the predicted values (COV 26 %). This can be mainly attributed to the lack of extensive diagonal
4 cracking in the retrofitted specimens and thus lower engagement of the bed joint reinforcement
5 during the tests. Therefore, for design purposes, verification of the lateral resistance in
6 reinforced cantilever walls should be carried out analysing both shear and flexural behaviour
7 and the minimum resistance should be used.

8
9
10
11
12
13
14
15 It becomes evident that, despite having a beneficial effect on the ductility, helical bars did not
16 substantially contribute to the lateral load resistance of cantilever masonry walls; similar results
17 have been reported in other studies [22] dealing with near-surface mounted bed joint steel
18 reinforcement. However, the presence of vertical “wiggled” or straight bars or even bed joint
19 bars alone was sufficient to effectively control shear cracking in the walls and prevent brittle
20 failure, which can greatly improve the safety of the masonry structures during seismic events.
21
22
23
24
25
26
27
28
29
30
31
32
33
34
35
36
37
38
39
40
41
42
43
44
45
46
47
48
49
50
51
52
53
54
55
56
57
58
59
60
61
62
63
64
65
Due to their flexibility and relatively high tensile capacity, the use of helical bars improved the
post-peak in-plane behaviour allowing reinforced masonry to undergo larger drift levels and
dissipate more hysteretic energy. Being able to accommodate larger displacement demands the
retrofitted walls showed that ductility improved by up to 146 % compared to the reference
walls. This also resulted in behaviour factors larger than 4.0, which exceeds typical factors for
reinforced masonry and seem to be in similar range to the factors derived for retrofitted masonry
(e.g. [19]), however, this observation should be treated with caution as this very much depends
how the yield displacement of the wall is defined.

5. Conclusions

The paper investigated, for the first time, the potential of helical bars as seismic reinforcement
for unreinforced masonry piers. A total of nine masonry cantilever walls were subjected to
quasi-static cyclic loading until failure associated with about 25 % load drop. Various
retrofitting layouts were investigated, exploring the use of horizontal and vertical straight and

vertical “wiggled” bars (a novel type of combined horizontal and vertical reinforcement feasible due to the flexibility of the helical bars) as well as bed joint bars. The experimental results were assessed in terms of strengthening efficiency, ductility, and energy dissipation; and were verified using Eurocode 6 provisions for masonry structures. Based on the experiments and analysis discussed above, the following conclusions can be drawn:

- Tensile tests showed that 6 mm helical bars have different characteristics than regular steel bars. Due to the specific production process, helical reinforcement can undergo larger deformations whilst maintaining relatively large stress levels, and the stress-strain relationship is characterised by a not well-defined yield point. The tests revealed an average tensile strength equal to 1181 MPa, 0.2% proof strength of 917 MPa and elastic range limit at a level of about 455 MPa. This greatly exceeds the typical stress levels in standard 6 mm steel rebars, which usually start yielding at stress levels around 500 MPa at 0.2 % deformation.
- Having initially experienced rocking at the base, the cantilever URM walls subsequently failed in shear and had very limited energy dissipation. The wall with higher vertical stress level exhibited diagonal shear cracks in both loading directions, whereas the wall with lower stress level, after significant rocking, failed by shear sliding (showing also signs of diagonal cracking). The walls retrofitted with helical bars did not exhibit shear failure, but a more controlled flexural failure related to rocking, which was terminated by compressive capacity of the bricks in the toe regions.
- The retrofitted walls did not show any significant increase in lateral load resistance compared to URM walls even in the case that vertical bars were added at the wall edges. However, the post peak performance of the retrofitted walls was significantly improved, and some residual lateral load capacity was maintained.
- The walls reinforced with helical bars exhibited larger ductility than the bare walls and the former should develop more gradual and more controlled failure. The behaviour

factors for retrofitted walls significantly increased compared to the factors for URM walls and exceeded the typical values for reinforced masonry as specified in Eurocode. Hence, such a retrofitting system has the potential to offer additional deformation capacity to the masonry and maintain the integrity of the walls, even when severe in-plane damage is developed. Concluding, the use of helical bars has the potential to increase the life-safety performance of the masonry structures during seismic actions without much interference in the aesthetics of masonry.

- The Eurocode 6 provisions and experimentally-derived material characteristics were sufficient to reasonably predict the lateral load capacity of URM and retrofitted walls. The diagonal cracking and shear sliding failures were predicted with experimental-to-theoretical ratios equal to 0.99 and 1.29, respectively. The flexural failure of retrofitted walls was estimated considering flexural contributions of masonry and helical reinforcement and resulted in an average ratio of 1.07 suggesting that Eurocode 6 provisions can be directly applied for load capacity estimations, although they do not explicitly account for the effects of cyclic degradation.

It is believed that the true potential of stainless-steel helical bars for as a seismic reinforcement was not fully explored in this study due to the fact that only cantilevers were investigated, and such structures do not usually show extensive shear cracking, and therefore, do not fully engage horizontal reinforcement. Past research studies on masonry wallettes with bed joint helical bars [32, 34] demonstrated that helical bed reinforcement can be very effective in bridging diagonal cracks and can lead to a substantial increase in shear strength and in-plan deformation capacity. It is deemed that future research on the use of helical reinforcement for seismic retrofitting should focus on cyclic static and dynamic tests on masonry piers and spandrels with fixed-fixed boundary conditions, which more accurately represent shear-critical masonry piers during earthquakes and can promote diagonal cracks, hence better exploiting the potential of bed joint helical reinforcement.

Nevertheless, helical reinforcement has a clear potential to preserve integrity of the structure and increase safety of masonry buildings during earthquakes with minimum installation efforts and without changing visual aesthetics of the walls.

Acknowledgments

This research was funded through Knowledge Transfer Partnership (KTP011576). The authors would like to thank Innovate UK and Target Fixings Ltd (manufacturer of helical reinforcement Bar Flex) for financing the project and City, University of London wherein the experimental work has taken place.

References

- [1] Matthys, H., Noland, L. Strengthening and retrofitting masonry buildings. In Proceedings of the An International Seminar on Evaluation, Strengthening and Retrofitting Masonry Buildings, TMS, Boulder, CO, USA, 11–18 October 1989.
- [2] Abrams, D. P. (1992). Strength and behavior of unreinforced masonry elements. In Proceedings of the 10th World Conference on Earthquake Engineering, Madrid (Balkema); 3475-3480.
- [3] Anthoine, A., Magonette, G., & Magenes, G. (1995). Shear-compression testing and analysis of brick masonry walls. In Proceedings of the 10th European Conference on Earthquake Engineering. Vol. 3, pp. 1657-1662.
- [4] Tomaževič, M., Lutman, M., & Petković, L. (1996). Seismic behavior of masonry walls: experimental simulation. *Journal of structural engineering*, 122(9), 1040-1047.
- [5] Magenes, G., & Calvi, G. M. (1997). In-plane seismic response of brick masonry walls. *Earthquake engineering & structural dynamics*, 26(11), 1091-1112.
- [6] Tomaževič, M. (1999). *Earthquake-resistant design of masonry buildings (Vol. 1)*. World Scientific.
- [7] Priestley, M. J. N. (1985). Seismic behaviour of unreinforced masonry walls. *Bulletin of the New Zealand Society for Earthquake Engineering*, 18(2), 191-205.
- [8] Wallemacq, P., and R. House. 2018. “UNISDR and CRED report: Economic Losses, Poverty and Disasters (1998–2017), United Nations Office for Disaster Risk Reduction (UNISDR) and the Centre for Research on the Epidemiology of Disasters (CRED).” Accessed March 5, 2021. <http://www.emdat.be/publications>.
- [9] Taghdi, M., Bruneau, M., & Saatcioglu, M. (2000). Seismic retrofitting of low-rise masonry and concrete walls using steel strips. *Journal of Structural Engineering*, 126(9), 1017-1025.
- [10] Farooq, S. H., ElGawady Mohamed, A., & Ilyas, M. (2014). Seismic in-plane performance of retrofitted masonry walls. *KSCE Journal of Civil Engineering*, 18, 226-237.
- [11] Ashraf, M., Khan, A. N., Naseer, A., Ali, Q., & Alam, B. (2012). Seismic behavior of unreinforced and confined brick masonry walls before and after ferrocement overlay retrofitting. *International Journal of Architectural Heritage*, 6(6), 665-688.
- [12] Churilov, S., & Dumova-Jovanoska, E. (2013). In-plane shear behaviour of unreinforced and jacketed brick masonry walls. *Soil Dynamics and Earthquake Engineering*, 50, 85-105.
- [13] Shermi, C., & Dubey, R. N. (2018). In-plane behaviour of unreinforced masonry panel strengthened with welded wire mesh and mortar. *Construction and Building Materials*, 178, 195-203.

- [14] Stratford, T., Pascale, G., Manfroni, O., & Bonfiglioli, B. (2004). Shear strengthening masonry panels with sheet glass-fiber reinforced polymer. *Journal of Composites for Construction*, 8(5), 434-443.
- [15] El Gawady, M. A., Lestuzzi, P., & Badoux, M. (2007). Static cyclic response of masonry walls retrofitted with fiber-reinforced polymers. *Journal of composites for Construction*, 11(1), 50-61.
- [16] Rahman, A., & Ueda, T. (2016). In-plane shear performance of masonry walls after strengthening by two different FRPs. *Journal of composites for construction*, 20(5), 04016019.
- [17] Papanicolaou, C. G., Triantafillou, T. C., Karlos, K., & Papanasiou, M. (2007). Textile-reinforced mortar (TRM) versus FRP as strengthening material of URM walls: in-plane cyclic loading. *Materials and structures*, 40, 1081-1097.
- [18] Papanicolaou, C., Triantafillou, T., & Lekka, M. (2011). Externally bonded grids as strengthening and seismic retrofitting materials of masonry panels. *Construction and Building Materials*, 25(2), 504-514.
- [19] Trochoutsou, N., Di Benedetti, M., Pilakoutas, K., & Guadagnini, M. (2022). In-Plane Cyclic Performance of Masonry Walls Retrofitted with Flax Textile-Reinforced Mortar Overlays. *Journal of Composites for Construction*, 26(5), 04022049.
- [20] Cholostiakow, S., Koutas, L. N., & Papakonstantinou, C. G. (2023). Geopolymer versus cement-based textile-reinforced mortar: Diagonal compression tests on masonry walls representative of infills in RC frames. *Construction and Building Materials*, 373, 130836.
- [21] Valluzzi, M. R., Binda, L., & Modena, C. (2005). Mechanical behaviour of historic masonry structures strengthened by bed joints structural repointing. *Construction and building materials*, 19(1), 63-73.
- [22] Soti, R., & Barbosa, A. R. (2019). Experimental and applied element modeling of masonry walls retrofitted with near surface mounted (NSM) reinforcing steel bars. *Bulletin of Earthquake Engineering*, 17, 4081-4114.
- [23] Tumialan, G., Huang, P. C., Nanni, A., & Silva, P. (2001, July). Strengthening of masonry walls by FRP structural repointing. In *Proc., 5th Int. Conf. on Fibre Reinforced Plastics for Reinforced Concrete Structures*, Thomas Telford, Cambridge, UK (pp. 1033-1042).
- [24] Li, T., Galati, N., Tumialan, J. G., & Nanni, A. (2005). Analysis of unreinforced masonry concrete walls strengthened with glass fiber-reinforced polymer bars. *ACI structural journal*, 102(4), 569.
- [25] Konthesingha, K. M. C., Masia, M. J., Petersen, R. B., & Page, A. W. (2015). Experimental evaluation of static cyclic in-plane shear behavior of unreinforced masonry walls strengthened with NSM FRP strips. *Journal of Composites for Construction*, 19(3), 04014055.
- [26] Parvin, A., & Syed Shah, T. (2016). Fiber reinforced polymer strengthening of structures by near-surface mounting method. *Polymers*, 8(8), 298.
- [27] Paulay, T. and Priestley, M.J.N. (1992) *Seismic Design of Reinforced Concrete and Masonry Buildings*. J. Wiley & Sons, New York.
- [28] Abrams, D.P., "Performance Based Engineering Concepts for Unreinforced Masonry Building Structures, *Progress in Structural Engineering and Materials*, Vol. 3, No. 1, 2001, pp. 48-56.
- [29] Gentilini, C., Finelli, F., Girelli, V. A., & Franzoni, E. (2021). Pull-out behavior of twisted steel connectors employed in masonry: The influence of the substrate. *Construction and Building Materials*, 274, 122115.
- [30] Gentilini, C., Finelli, F., & Carloni, C. (2022). An experimental study of the bond behavior of twisted steel bars embedded in mortar cylinders and in the joints of masonry wallettes. *Construction and Building Materials*, 316, 125795.
- [31] Cattaneo, S., & Scamardo, M. (2023). Assessment of the tensile behavior of twisted steel connectors for masonry retrofitting. *Construction and Building Materials*, 392, 131771.
- [32] Ismail, N., Petersen, R. B., Masia, M. J., & Ingham, J. M. (2011). Diagonal shear behaviour of unreinforced masonry wallettes strengthened using twisted steel bars. *Construction and building materials*, 25(12), 4386-4393.

- [33] Cattaneo, S., Crespi, P., Scamardo, M., & Vafa, N. (2023). Cyclic behavior of masonry walls retrofitted with post-installed twisted bars or bonded rebars. *Construction and Building Materials*, 409, 134026.
- [34] Petersen, R. B., Ismail, N., Masia, M. J., & Ingham, J. M. (2012). Finite element modelling of unreinforced masonry shear wallettes strengthened using twisted steel bars. *Construction and Building Materials*, 33, 14-24.
- [35] Petry, S., & Beyer, K. (2014). Influence of boundary conditions and size effect on the drift capacity of URM walls. *Engineering structures*, 65, 76-88.
- [36] RILEM. (1991). "Diagonal tensile strength tests of small wall specimens." TC 76-LUM, Bagneux, France.
- [37] CEN (2019). EN 1015. Methods of test for mortar for masonry – Part 11: Determination of flexural and compressive strength of hardened mortar. European Committee for Standardization, Brussels.
- [38] CEN (1998). EN 1052. Methods of tests for masonry—Part 1: Determination of compressive strength.
- [39] CEN (2002). EN 1052. Methods of test for masonry—Part 3: Determination of initial shear strength.
- [40] ISO (2019). ISO 6892. Metallic materials — tensile testing — Part 1: Methods of test at room temperature.
- [41] Abrams, D., Smith, T., Lynch, J., & Franklin, S. (2007). Effectiveness of rehabilitation on seismic behavior of masonry piers. *Journal of Structural Engineering*, 133(1), 32-43.
- [42] CEN (2005a). EN 1998. Eurocode 8. Design of structures for earthquake resistance - Part 3. Brussels, Belgium.
- [43] CEN (2004). EN 1998. Eurocode 8. Design of structures for earthquake resistance - Part 1. Brussels, Belgium.
- [44] FEMA (2000). Prestandard and commentary for the seismic rehabilitation of buildings. FEMA 356. Washington, DC
- [45] ASTM (2019). E 2126. Standard test methods for cyclic (reversed) load test for shear resistance of vertical elements of the lateral force resisting systems for buildings. West Conshohocken, PA.
- [46] Bosiljkov, V., Page, A. W., Bokan-Bosiljkov, V., & Žarnić, R. (2010). Evaluation of the seismic performance of brick masonry walls. *Structural Control and Health Monitoring: The Official Journal of the International Association for Structural Control and Monitoring and of the European Association for the Control of Structures*, 17(1), 100-118.
- [47] CEN (2005a). EN 1996. Eurocode 6. General rules for reinforced and unreinforced masonry structures - Part 1-1. Brussels, Belgium.
- [48] DIN (2011). DIN EN 1996. Eurocode 6/NA. General rules for reinforced and unreinforced masonry structures - Part 1-1/National Annex. Germany.
- [49] Mann, W., & Müller, H. (1982). Failure of shear stressed masonry. An enlarged theory, tests and application to shear walls. *Proceedings of the British Ceramic Society*, 30, 223–235.
- [50] Petersen RB (2009). In-plane shear behaviour of unreinforced masonry panels strengthened with fibre reinforced polymer strips. *PhD thesis*, University of Newcastle, Newcastle, Australia.
- [51] Turnšek V, Čačovič F. (1971). Some experimental results on the strength of brick masonry walls. In: *Proceedings of the second international brick-masonry conference*, British Ceramic Society, Stoke-on-Trent, 149–156.